Giant Friedel Oscillations on the Beryllium(0001) Surface

P. T. Sprunger,*† L. Petersen, E. W. Plummer, E. Lægsgaard, F. Besenbacher

Large-amplitude electron density oscillations were observed on a Be(0001) surface by means of variable-temperature scanning tunneling microscopy. Fourier transforms of the images showed a ring of radius $2k_F$, where k_F is the Fermi wave vector of the Be(0001) surface state. This wavelength was expected from Friedel oscillations caused by electronic screening of surface defects, but the amplitude of the waves for energies near the Fermi energy was anomalously large and inconsistent with the Friedel concept of screening. The enhanced amplitude of the waves must be a many-body effect, either in the electron gas (possibly an incipient charge density wave) or in the response of the lattice (electron-phonon coupling).

One of the fundamental concepts of solid-state physics is screening, that is, the ability of a material to rearrange its electron sea in order to minimize the disturbance of an impurity or defect. Friedel showed that screening of a point-charged impurity in the bulk results in long-range oscillatory behavior in the charge density (*1*). For simple free-electron–like metals, these oscillations have a wave vector of $2k_F$ [where k_F is the wave vector of a Fermi energy (E_F) electron] as a consequence of the sharp Fermi surface in a metal ($E_F = \hbar^2k_F^2/2m$, where $\hbar$ is Planck's constant divided by 2π and m is the electron effective mass). At a metal surface, this screening phenomenon results in an oscillation in the charge density perpendicular to the surface (*2*) as well as a lateral disturbance from impurities (*3*, *4*) or steps. Friedel oscillations constitute the mechanism for long-range interaction in metals. For example, in catalytic processes, the indirect interaction between adsorbed atoms or molecules on a surface is a direct consequence of screening, that is, the Friedel oscillations (*3*, *4*). It is also likely that step-step interaction at a metal surface is mediated by Friedel oscillations, with implications for epitaxial growth. Finally, long-range screening dictates many interface magnetic properties because of the spin-dependent exchange interaction (*5*); this effect is responsible for the coupling of thin magnetic films in which giant magnetoresistance phenomena have recently been observed (*6*).

Although it has proven difficult to access Friedel oscillations directly in the bulk, at a surface scanning tunneling microscopy (STM) (*7*) gives a direct image of the charge corrugation (*8*–*11*). Crommie *et al.* (*8*) and Hasegawa *et al.* (*9*) imaged standing waves originating at steps and impurities on the (111) faces of noble metals. These standing waves are the energy-resolved Friedel oscillations, because in general the bias on the scanning tunneling microscope is small relative to the bandwidth. Friedel oscillations have also been observed surrounding Ar bubbles in aluminum (*10*) and even for Si dopants in a semiconductor (*11*). In general, these are not primarily two-dimensional (2D) systems because the electronic states at the surface are strongly coupled to the bulk states, which leads to appreciable scattering of the surface waves into bulk states (*11*).

Here, we report on giant Friedel oscillations (*12*) on the Be(0001) surface. Our motivation for studying this system was to explore the nature of Friedel oscillations in a truly 2D system. Because the exchange and correlation energies, relative to the kinetic energy, are considerably larger in a 2D than in a 3D system, we hypothesized that many-body enhancement or stabilization of the screening oscillations was possible (*13*). This expectation was correct (Fig. 1). Giant amplitude electron density waves dominate the constant-current STM images to the extent that only waves are visible—a true electron sea, with the atomic lattice totally hidden. We contend that the large amplitude of the waves shown in Fig. 1 is inconsistent with Friedel's single-particle concept of screening.

Friedel solved the screening problem by deriving a sum rule on the scattering phase shifts necessitated by charge neutrality (*1*, *14*). A more intuitive approach is to use dielectric response theory, where the static dielectric constant $\varepsilon(\mathbf{q})$ is used to screen the impurity or defect potential $V_o(\mathbf{r})$. The 3D screened potential is given by

$$V_{sc}(\mathbf{r}) = \int d^3\mathbf{q} V_{oq} \exp(i\mathbf{qr})/\varepsilon(\mathbf{q}) \quad (1)$$

where V_{oq} is the Fourier transform (FT) of $V_o(\mathbf{r})$. The induced potential is given by $V_{ind}(\mathbf{r}) = V_{sc}(\mathbf{r}) - V_o(\mathbf{r})$, and the induced charge density, $\rho_{ind}(\mathbf{r})$, can be determined from $V_{ind}(\mathbf{r})$ with Poisson's equation, $\nabla^2 V_{ind}(\mathbf{r}) = -4\pi e\, \rho_{ind}(\mathbf{r})$ (where e is the electron charge) or, more generally in a linear-response approach, from the FTs of the screened potential and the static dielectric susceptibility $\chi(\mathbf{q})$, namely, $\rho_{ind}(\mathbf{q}) = \chi(\mathbf{q})V(\mathbf{q})$. These representations of the induced screening charge also allow for a straightforward evaluation of the effects of dimensionality on the nature of the impurity potential and on the dielectric response. For example, although the relation between the static dielectric constant and the susceptibility for a 3D impurity is $\varepsilon(\mathbf{q}) = 1 - 4\pi\, \chi(\mathbf{q})/q^2$, for a 2D impurity the relation is $1 - 2\pi\, \chi(\mathbf{q})/q$. This changes the functional form of the induced charge density. If the Lindhard response function (*15*) is used, the 3D asymptotic limit for large r gives an induced charge density from a point impurity of the form

$$\rho(r) = A[\cos(2k_F r + \phi)]/r^3 \quad (2)$$

where A is amplitude and ϕ is a phase shift associated with the scattering potential. The long-range oscillations are caused by the singularity in the derivative of the Lindhard dielectric function at $q = 2k_F$ (*14*, *16*). Both the Friedel scattering approach and the Lindhard dielectric response approach are based on single-particle concepts (*14*).

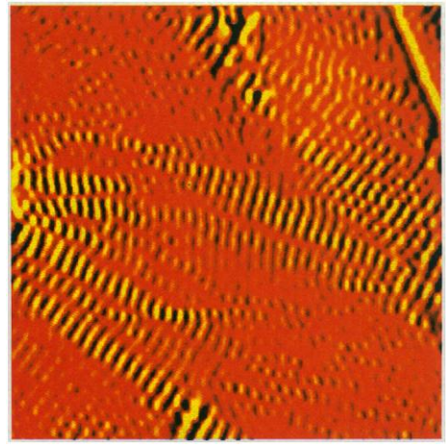

Fig. 1. Constant-current STM image (110 Å by 110 Å, $I = -0.84$ nA, $V = -3.7$ mV) of Be(0001) at 150 K, showing impurity and defect effects on waves.

P. T. Sprunger, L. Petersen, E. Lægsgaard, F. Besenbacher, Institute of Physics and Astronomy, University of Aarhus and Center for Atomic-Scale Materials Physics, DK-8000 Aarhus C, Denmark.
E. W. Plummer, Department of Physics and Astronomy, University of Tennessee, Knoxville, TN 37996, USA, and Solid State Division, Oak Ridge National Laboratory, Oak Ridge, TN 37831, USA.

*Present address: Center for Advanced Microstructures and Devices, Louisiana State University, Baton Rouge, LA 70803, USA.
†To whom correspondence should be addressed. E-mail: sprunger@camd.lsu.edu

Reductions in dimensionality affect the response of the system to an impurity. The wavelength of the oscillatory component of the charge density is a consequence of the singularity in the dielectric response at $q = 2k_F$, which is present for all dimensions (*17*). However, the amplitude and the power law fall-off shown in Eq. 2 both depend on the dimensionality of the impurity and the dielectric response. For example, the surface is a 2D defect embedded in a 3D electron gas. Friedel oscillations emanate from the surface into the bulk with an asymptotic form of $1/r^2$ (*2*, *18*). Fermi surface nesting in two dimensions can lead to the stabilization of charge density waves (CDWs) (*17*, *19*), and in the extreme case of a 1D system, the Lindhard static dielectric susceptibility $\chi(\mathbf{q})$ has a logarithmic singularity at $q = 2k_F$, which leads to a giant Kohn anomaly (*20*) in the phonon dispersion at $2k_F$ and an instability resulting in a Peierls distortion of the lattice (*21*).

For a true 2D system, the character of the singularity in the susceptibility is more profound than the 3D case but is not as extreme as the 1D case (*17*). The functional form of the susceptibility, as calculated by Stern (*22*), shows a singularity in the first derivative at $q = 2k_F$. However, the possibility exists that many-body effects will dominate the 2D response (*13*). For example, it has been predicted that a 2D electron gas with a density $\sim$<80% of the density of Al ($r_s > 2.2$) is unstable (negative compressibility) (*23*), which has been confirmed for electrons in a modulation-doped GaAs-AlGaAs heterostructure (*24*). There is even a prediction that the Friedel oscillations for a 2D system are so stabilized by exchange and correlation that they lead to a Bose-Einstein condensation for $r_s > 2$ (*25*).

As outlined above, the nature of the Friedel waves is expected to be quite different in a 2D versus a 3D system. Our choice of the Be(0001) surface was motivated by its unusual properties (*26*). Previous structural, electronic, and dynamic studies have shown that this surface is a nearly ideal 2D free-electron system because of the high density of surface states, whereas the underlying bulk is almost a semiconductor. The surface states are localized within ~2 Å of the surface, and the 2D density of states (DOS) at E_F is five times the corresponding bulk density (*25*). Therefore, the electronic character of the (0001) surface of Be should behave as a high-density 2D electron gas on a nearly semiconducting substrate.

We observed enhanced surface Friedel waves on Be(0001) with a high-stability scanning tunneling microscope (*27*) capable of operating at temperatures from 120 to 370 K. The microscope was installed in an ultrahigh-vacuum chamber ($P < 10^{-10}$ mbar) equipped with standard facilities for surface cleaning and characterization. All of the STM images presented here were recorded in the constant-current mode with single-crystal tungsten tips. The final crystal cleaning procedure included repeated cycles of room-temperature 1.5-keV Ne^+ sputtering and subsequent annealing to 725 K. At the end of the cleaning cycle, (1 × 1) low-energy electron diffraction (LEED) patterns were quite sharp with low background. Auger electron spectroscopy showed very small amounts of contaminants (oxygen, carbon, and subsurface neon, all at or below 1.5% of a monolayer).

The constant-current image in Fig. 1 represents the local DOS at E_F, $n(E_F,\mathbf{r})$, with the total charge density given by $\rho(\mathbf{r}) = \int en(E,\mathbf{r})dE$. The large amplitude of the Friedel oscillations (*12*) on Be(0001) is apparent in Fig. 1, where the charge corrugation is ~0.3 Å, compared with ~0.02 Å corrugation reported for the Friedel oscillations on Cu(111) with a bias voltage of 0.02 V (*8*). The waves dominate the surface topography, and their short wavelength (3.2 Å) is comparable to atomic distances. This wavelength is much shorter than that seen on the noble metal (111) surfaces (~15 Å), and their amplitude is largest near surface impurities or defects, which is as expected because the waves are a result of the screening of these areas. In Fig. 2A, the surface is dominated by a complex interference pattern of short-wavelength surface Friedel waves. The pattern cannot be accounted for by a single plane or circular wave. In the present case, the waves are virtually undamped on the scale of many wavelengths (*28*).

The FT of the image in Fig. 2A is shown in Fig. 2B. Comparison of Fig. 2B with the 2D Fermi surface of Be(0001) (Fig. 2C) reveals that the ring identified in the FT-STM image has twice the radius of the surface state of the 2D Fermi surface ($2k_F$ versus k_F). The 2D Fermi surface for the surface states and the projection of the bulk Fermi surface (Fig. 2C) show that there is a well-defined 2D Fermi surface created by the abundance of surface states, as well as a small projection of the bulk Fermi surface onto the surface Brillouin zone. The 2D reciprocal lattice vectors **G** and the ring associated with $2k_F$ are also shown in Fig. 2C. The surface Fermi wave vector k_F is large in this case, so that the wavelength of the surface wave is short [3.2 Å, compared with a wavelength of 16 Å seen on Au (*9*)]. An interesting feature revealed in the FT-STM image (Fig. 2B) is the hexagonal array of weak intensity spots, corresponding to the Be reciprocal lattice (2.27 Å). Even though the Be lattice cannot be "seen" in the STM image, it is nonetheless identified in the FT. These spots in the FT are the reciprocal lattice vectors **G** (Fig. 2C). Thus, the FT-STM image represents a combined structural and electronic measurement, containing the information obtained from both LEED and angle-resolved photoemission spectroscopy. An FT-STM image directly produces a "picture" of the 2D Fermi surface, calibrated by the presence of the reciprocal lattice vectors **G**. The surface wave vector determined from 72 different images is 1.89 ± 0.04 $Å^{-1}$. This value compares very well with photoemission data, which determined the k_F of the surface state to be 0.93 $Å^{-1}$ in the $\overline{\Gamma} \rightarrow \overline{K}$ direction and 0.96 $Å^{-1}$ in the $\overline{\Gamma} \rightarrow \overline{M}$ direction (average $2k_F$ = 1.89 $Å^{-1}$) (*26*).

Another characteristic of the electron density waves on Be is that the amplitude is gigantic only for electrons near the Fermi energy (Fig. 3). The electron density corrugation for the image taken with a bias voltage of –2.1 mV (Fig. 3C) is 0.42 Å, whereas the corrugation decreases by an order of magnitude when the bias voltage is increased to –35 mV (Fig. 3B). Measurements on Cu(111) showed a corrugation of ~0.02 Å (*8*). To understand how unusual this behavior is, it is necessary to return to

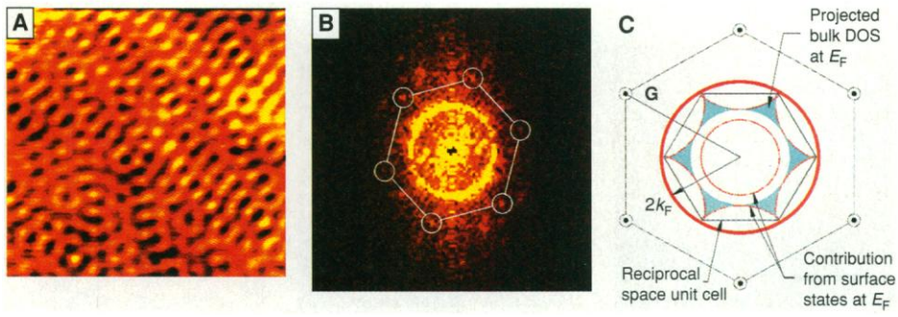

Fig. 2. (**A**) Constant-current STM image (40 Å by 40 Å, I = 1.5 nA, V = 4 mV) of Be(0001) at 150 K. (**B**) The 2D FT of the image in (A). (**C**) The 2D Brillouin zone of Be(0001) in which the circles (shaded region) correspond to the surface states (projected bulk bands) at E_F. The reciprocal space unit cell with the corresponding $2k_F$ "ring" is also shown.

single-particle scattering theory. The energy-resolved Friedel oscillation (8, 9) is defined as the local density of electronic states $n(E,\mathbf{r})$. For a line defect in a 2D system, $\Delta\rho(E,\mathbf{r}) \propto g_o[\cos(2kr + \phi)]/r^{1/2}$ (9), where k is the wave vector associated with an electron at energy E and g_o is the 2D local electronic DOS [which is a constant, independent of the energy or wave vector for free electron dispersion (15)]. This predicted behavior for energy-resolved Friedel oscillations is almost exactly what Crommie *et al.* (8) observed in their low-temperature STM images of Cu(111). In contrast, the waves on Be have a profound energy dependence that is totally inconsistent with the single-particle concept of screening. The enhanced amplitude of the waves must be caused by a many-body effect, either in the electron gas (possibly an incipient CDW) (29) or in the response of the lattice (electron-phonon coupling) (13, 15).

Overhauser's work (29) implies that a 2D electron gas will have a greater tendency to form a CDW than will a 3D electron gas. Naïvely, a CDW would be expected to appear in the STM images as a charge density corrugation independent of the bias voltage. A possible explanation of the remarkably high amplitude of the waves near E_F consistent with the CDW concept has been proposed (30). For this hexagonal structure there could be three CDW vectors (adding to a null vector) with a magnitude close to that of $2k_F$. The consequence of the CDW in terms of a band picture would be the formation of a gap, with the gap pinned at the Fermi energy. The DOS in a strictly 2D picture is divergent at the lower edge of the gap and discontinuous at the upper edge (30). With respect to our data, this could account for the very large intensity of the observed waves, given that the E_F is pinned to the lower band edge.

A second tentative explanation involves electron-phonon coupling at the surface. If the 2D nature of the Be(0001) surface enhances the electron-phonon coupling, then there will be a distortion of the electronic bands at E_F (16). This distortion increases the DOS at E_F by a factor of $1 + \lambda$ (where λ is the electron-phonon coupling constant) and decreases the DOS at energies that are a fraction of the phonon bandwidth above or below E_F [see figure 26.1 of (16)]. The phonon bandwidth in Be is 0.084 eV (26). An appreciable enhancement in λ at the surface of Be may be consistent with observations of superconductivity in Be. Crystalline Be has a superconducting transition temperature $T_c = 0.026$ K (31), but in the amorphous state the temperature increases by a factor of nearly 400 [$T_c = 9.6$ K (32)], making it the highest recorded elemental T_c value. This fact is not understood; however, it could be reconciled with our results if there is a large λ at surfaces and interfaces.

Experimental tests of these two models would include examining the temperature dependence of the Friedel waves through a more extended range (33), determining the inherent coherence length of the waves (28), and investigating the effect of modifying the Fermi surface, either by adsorption (26) or alloying (30). High-resolution angle-resolved photoemission should also be able to probe the properties of the 2D Fermi surface on Be(0001).

In light of the observations discussed above, it is useful to speculate about the use of Be(0001) in future experiments. Be(0001) may be uniquely tailored to study such effects as electron-phonon coupling, long-range oscillatory adatom-adatom interactions, and periodic lattice distortions. Because there should be appreciably less scattering of the surface wave into the bulk for Be relative to most other metals, real quantum corrals could be constructed where the reflection probability could be appreciably greater than in previously studied systems (34). The large magnitude of the surface waves could also be used to order adsorbates on a surface of Be and investigate the effect of the 2D Fermi surface on the adatom-adatom interaction (4). Also, it is conceivable that this incommensurate electron density oscillation will create a lattice distortion. The inconsistency between the 5.8% and 2.7% expansion of the Be(0001) surface plane determined experimentally (35) and theoretically (36) could be a consequence of the fact that the incommensurate lattice distortion caused by the Friedel oscillations has been ignored.

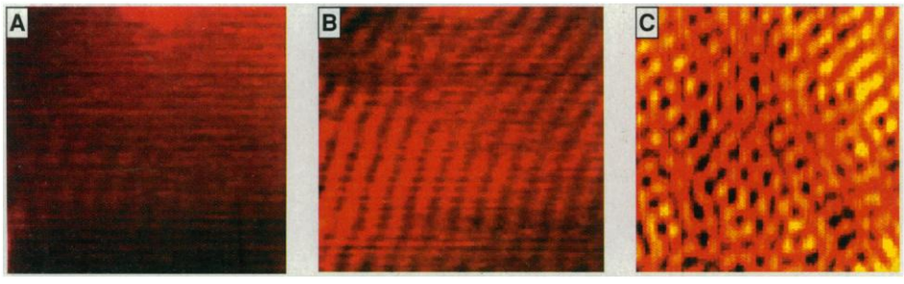

Fig. 3. STM images (50 Å by 50 Å) of Be(0001) at 150 K for different tunneling voltages. (**A**) $V = -116$ mV, $I = 2.87$ nA; corrugation, 0.028 Å. (**B**) $V = -35$ mV, $I = -2.24$ nA; corrugation, 0.042 Å. (**C**) $V = -2.1$ mV, $I = -0.92$ nA; corrugation, 0.42 Å. The change of the wavelength of the surface state corresponding to 116 mV is 1.4%, below our resolution.

REFERENCES AND NOTES

1. J. Friedel, *Nuovo Cimento Suppl.* **7**, 287 (1958).
2. N. D. Lang and W. Kohn, *Phys. Rev. B* **1**, 4555 (1970).
3. T. L. Einstein and J. R. Schrieffer, *ibid.* **7**, 3629 (1973).
4. K. H. Lau and W. Kohn, *Surf. Sci.* **75**, 69 (1978).
5. M. A. Ruderman and C. Kittel, *Phys. Rev.* **96**, 99 (1954).
6. M. D. Stiles, *Phys. Rev. B* **48**, 7238 (1993).
7. G. Binnig and H. Rohrer, *Helv. Phys. Acta* **55**, 726 (1982).
8. M. F. Crommie, C. P. Lutz, D. M. Eigler, *Nature* **363**, 524 (1993); E. J. Heller, M. F. Crommie, C. P. Lutz, D. M. Eigler, *ibid.* **369**, 464 (1994); in *The Physics of Electronic and Atomic Collisions*, L. J. Dube, J. B. Mitchell, J. W. McConkey, C. E. Brion, Eds. (AIP Press, Woodbury, NY, 1995), pp. 3–17.
9. Y. Hasegawa and Ph. Avouris, *Phys. Rev. Lett.* **71**, 1071 (1993); Ph. Avouris, I.-W. Lyo, R. E. Walkup, Y. Hasegawa, *J. Vac. Sci. Technol.* **B12**, 1447 (1994).
10. M. C. M. M. van der Wielen, A. J. A. van Roij, H. van Kempen, *Phys. Rev. Lett.* **76**, 1075 (1996).
11. M. Schmid, W. Hebenstret, P. Varga, S. Crampin, *ibid.*, p. 2298.
12. More correctly, the waves observed in STM images at low bias voltages are spectroscopically resolved Friedel oscillations; the actual Friedel oscillation represents the total charge density, that is, an energy integral over the occupied bandwidth.
13. A. K. Rajagopal and J. C. Kimball, *Phys. Rev. B* **15**, 2819 (1977).
14. G. D. Mahan, *Many-Particle Physics* (Plenum, New York, 1981).
15. J. Lindhard, *K. Dan. Vidensk. Selsk. Mat. Fys. Medd.* **28**, No. 8 (1954).
16. N. W. Ashcroft and N. D. Mermin, *Solid State Physics* (Holt, Rinehart and Winston, New York, 1976).
17. G. Grüner, *Density Waves in Solids* (Addison-Wesley, Reading, MA, 1994).
18. A. W. Overhauser, *Phys. Rev. B* **33**, 1468 (1986).
19. J. M. Carpinelli, H. H. Weitering, E. W. Plummer, R. Stumpf, *Nature* **381**, 398 (1996).
20. W. Kohn, *Phys. Rev. Lett.* **2**, 393 (1959).
21. R. E. Peierls, *Quantum Theory of Solids* (Oxford Univ. Press, Clarendon, UK, 1964).
22. F. Stern, *Phys. Rev. Lett.* **18**, 546 (1967).
23. B. Tanatar and D. M. Ceperley, *Phys. Rev. B* **39**, 5005 (1989).
24. J. P. Eisenstein, L. N. Pfeiffer, K. W. West, *Phys. Rev. Lett.* **68**, 674 (1992).
25. A. Gold, *Philos. Mag. Lett.* **70**, 141 (1994).
26. E. W. Plummer and J. B. Hannon, *Prog. Surf. Sci.* **46**, 149 (1994) and references therein; E. V. Chulkov, V. M. Silkin, E. N. Shirykalov, *Surf. Sci.* **188**, 287 (1987).
27. E. Lægsgaard, F. Besenbacher, K. Mortensen, I. Stensgaard, *J. Microsc.* **152**, 633 (1988); P. T. Sprunger, E. Lægsgaard, F. Besenbacher, *Phys. Rev. B* **54**, 8163 (1996).
28. Because of the relatively small terrace widths on our Be(0001) crystal and the complexity of the wave patterns, a characteristic decay length of the waves could not be directly determined. From FT-STM images, the k smearing Δk of the $2k_F$ "ring" was determined to be in the range $0.2 > \Delta k/k_F > 0.05$; however, the upper limit reflects the small size of many of the images.
29. A. W. Overhauser, *Phys. Rev. B* **2**, 874 (1970).
30. N. Ashcroft, personal communication.
31. L. I. Berger and B. W. Roberts, in *The CRC Handbook of Chemistry and Physics*, D. R. Lide, Ed. (CRC

Press, Boca Raton, FL, ed. 74, 1994), pp. 12–50.
32. R. E. Glover, R. Baumann, S. Moser, in *Proc. 12th Int. Conf. on Low Temp. Phys.*, E. Kanda, Ed. (Keigaku, Tokyo, 1971), p. 337.
33. Within our temperature range (150 to 300 K), there were no qualitative changes in the observations.
34. In the case of Fe on Cu, the iron atoms were modeled as absorbing "black dots" to correctly model the observed interference pattern (*8*).
35. H. L. Davis, J. B. Hannon, K. B. Ray, E. W. Plummer, *Phys. Rev. Lett.* **68**, 2632 (1992).
36. R. Stumpf and P. J. Feibelman, *Phys. Rev. B* **51**, 13748 (1995).
37. We thank N. Ashcroft, G. Mahan, A. Overhauser, E. Tossatti, and P. Feibelman for their contributions. Supported by NSF grant DMR-9510132 (E.W.P.) and the Center for Atomic-Scale Materials Physics (sponsored by the Danish National Research Foundation, the VELUX Foundation, and the Knud Højgaard Foundation).

18 November 1996; accepted 3 February 1997

Probing the Local Effects of Magnetic Impurities on Superconductivity

Ali Yazdani,* B. A. Jones, C. P. Lutz, M. F. Crommie,† D. M. Eigler

The local effects of isolated magnetic adatoms on the electronic properties of the surface of a superconductor were studied with a low-temperature scanning tunneling microscope. Tunneling spectra obtained near magnetic adsorbates reveal the presence of excitations within the superconductor's energy gap that can be detected over a few atomic diameters around the impurity at the surface. These excitations are locally asymmetric with respect to tunneling of electrons and holes. A model calculation based on the Bogoliubov–de Gennes equations can be used to understand the details of the local tunneling spectra.

Superconductivity and magnetism in solids occur because of dramatically different microscopic behaviors of electrons. In a superconductor, electrons form pairs with opposing spins, whereas to produce magnetism, electrons are required to have their spins aligned to form a net local magnetic moment. The competition between these effects manifests itself in the dramatic reduction of the superconducting transition temperature when magnetic impurities are introduced in a superconductor (*1*). Within the context of the pioneering theoretical work of Abrikosov and Gor'kov (*2*) and its extentions (*3*, *4*), a magnetic perturbation reduces the superconducting order parameter and leads to the appearance of quasiparticle excitations within the superconducting gap. Macroscopic planar tunnel junctions doped with magnetic impurities have shown sub-gap features in the superconductor's tunneling density of states (*5*). No direct measurement, however, has yet been reported on the structure of a magnetically induced quasi-particle excitation on the atomic length scale around a single magnetic impurity.

We directly probed the local electronic properties of a superconductor in the vicinity of a single, isolated magnetic atom with a scanning tunneling microscope (STM). We found that, near magnetic adatoms on the surface of a conventional superconductor, localized quasi-particle excitations at energies less than the superconductor's energy gap are induced in the superconductor by the impurities. Previously, the STM has been used to obtain local information on the nature of the electronic excitations of a vortex in a type II superconductor (*6*) on length scales comparable with the superconducting coherence length ξ_0. In contrast, the excitations reported here are detected over a few atomic diameters near the impurity, at length scales far shorter than ξ_0. We can explain the main features of our data with a model calculation of the local electronic properties of a magnetically doped superconductor based on the Bogoliubov–de Gennes equations; however, some features of the data remain unexplained.

We performed our experiments using an ultrahigh vacuum STM, which operates at temperatures down to $T = 3.8$ K. We used a single-crystal Nb(110) sample (99.999% purity) that was cleaned by numerous cycles of ion sputtering and vacuum annealing. Niobium samples of similar quality have bulk transition temperature $T_c \sim 9.2$ K, superconducting energy gap $2\Delta \sim 3.05$ meV, and $\xi_0 \sim 400$ Å. STM images of the sample after it had been processed and cooled to low temperatures showed the sample surface to be well ordered, with terraces as large as 100 Å, and to have an acceptable terrace defect density for our experiments. The main surface impurity was oxygen, which images as a dip in STM topographs. The local tunneling density of states (LDOS) of the Nb surface was obtained from measurement of the differential conductance dI/dV (where I is the current) of the STM junction versus sample bias voltage V (with respect to the tip) performed under open feedback loop conditions with standard low-frequency ac lock-in detection techniques. The width of the tunneling barrier (the height of the tip above the surface) during the measurements was adjusted before opening the feedback loop by setting the junction impedance R_j at an $eV \gg \Delta$. We used a polycrystalline Au wire as our tip; however, the chemical identity of the last atom on the tip is unknown.

We first measured the tunneling density of states for the Nb surface without the magnetic impurities. The spectrum in Fig. 1A is highly reproducible at different locations on the Nb surface, such as near atomic step edges and in the vicinity of surface defects such as oxygen. This spectrum can be fitted very well with the thermally broadened Bardeen-Cooper-Schrieffer (BCS) density of states (Fig. 1A) with a value of 2.96 meV for 2Δ, which is consistent with that reported for Nb, and a sample temperature of 3.85 K (*7*).

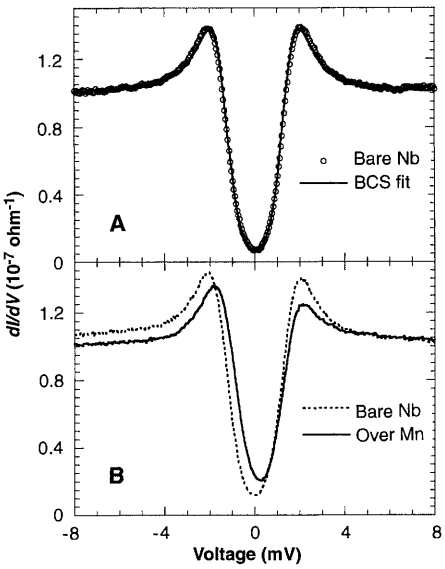

Fig. 1. (**A**) The dI/dV spectrum of the STM junction at $R_j = 10^7$ ohms ($V = 10$ mV) measured for the clean Nb(110) surface (open circles). The solid line is the BCS fit to the data. (**B**) Spectra measured ($R_j = 10^7$ ohm) near a Mn adatom. The solid line is from measurements with the tip over the adatom site and the dashed line is from measurements with the tip 16 Å away over the bare Nb surface. We used the convention that a positive bias V corresponds to electrons tunneling to the sample from the tip.

IBM Research Division, Almaden Research Center, 650 Harry Road, San Jose, Ca 95120, USA.

*To whom correspondence should be addressed. E-mail: yazdani@almaden.ibm.com

†Permanent address: Department of Physics, Boston University, Boston, MA 02215, USA.